53

GANIL

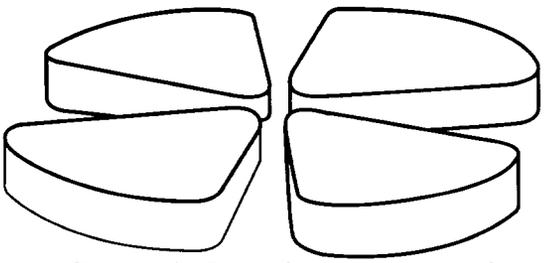

Quasielastic scattering of ^{8}B and ^{7}Be on ^{12}C at 40 MeV/nucleon

I.Pecina[1,5], R.Anne[1], D.Bazin[1], C.Borcea[2], V.Borrel[4], F.Carstoiu[2], J.M.Corre[1], Z.Dlouhy[5], A.Fomitchev[3], D.Guillemaud-Mueller[4], H.Keller[4], A.Kordyasz[6], M.Lewitowicz[1], S.Lukyanov[1,3], A.C.Mueller[4], Yu.Penionzhkevich[3], P.Roussel-Chomaz[1], M.G.Saint-Laurent[1], N.Skobelev[3], O.Sorlin[4], O.Tarasov[1,3]

[1] Grand Accelerateur National d'Ions Lourds, BP 5027, 14021 Caen Cedex, France
[2] Institute of Atomic Physics, P.O.Box MG6, 76900 Bucharest-Magurele Romania
[3] Flerov Laboratory of Nuclear Reactions, Joint Institute for Nuclear Research, 141980 Dubna, Moscow region, Russia
[4] Institut de Physique Nucléaire, CNRS-IN2P3, 91406 Orsay Cedex, France
[5] Nuclear Physics Institute, 250 68 Rez, Czech Republic
[6] Institute of Experimental Physics, Warsaw University, Hoza 69, 00681 Warsaw, Poland

GANIL P 94 22

Quasielastic scattering of ^{8}B and ^{7}Be on ^{12}C at 40 MeV/nucleon

I.Pecina[1,5], R.Anne[1], D.Bazin[1], C.Borcea[2], V.Borrel[4], F.Carstoiu[2], J.M.Corre[1], Z.Dlouhy[5], A.Fomitchev[3], D.Guillemaud-Mueller[4], H.Keller[4], A.Kordyasz[6], M.Lewitowicz[1], S.Lukyanov[1,3], A.C.Mueller[4], Yu.Penionzhkevich[3], P.Roussel-Chomaz[1], M.G.Saint-Laurent[1], N.Skobelev[3], O.Sorlin[4], O.Tarasov[1,3]

[1] Grand Accelerateur National d'Ions Lourds, BP 5027, 14021 Caen Cedex, France

[2] Institute of Atomic Physics, P.O.Box MG6, 76900 Bucharest-Magurele Romania

[3] Flerov Laboratory of Nuclear Reactions, Joint Institute for Nuclear Research, 141980 Dubna, Moscow region, Russia

[4] Institut de Physique Nucléaire, CNRS-IN2P3, 91406 Orsay Cedex, France

[5] Nuclear Physics Institute, 250 68 Rez, Czech Republic

[6] Institute of Experimental Physics, Warsaw University, Hoza 69, 00681 Warsaw, Poland

Abstract

The quasielastic scattering of the exotic nucleus ^{8}B on a ^{12}C target has been studied at an energy of 320 MeV and is compared with that of ^{7}Be at the same velocity. The $^{12}C+^{12}C$ quasielastic scattering at 20 MeV/nucleon, also performed as a secondary beam experiment, was used to check the data reduction method. The experimental data are compared with a semimicroscopic double folding model and coupled-channels calculation. The difference in the reaction cross section (8%) between ^{8}B and ^{7}Be corresponds to an increase in the interaction radius of 4%. The existence of proton halo in ^{8}B is not supported by the present data.

PACS number(s): 25.60.+v, 25.70.Bc

I. INTRODUCTION

Recently, the ^{8}B nucleus received much attention from both experimental and theoretical points of view. Its low proton separation energy of only 137 keV and the location of its last proton in a relative p-state with respect to the ^{7}Be core, suggest that ^{8}B could be a proton halo candidate [1]. Recent experiments provide contradictory information, pointing either towards a very large halo or to a vanishing one. In a recent experiment, Minamisono et al. [2] found an electric quadrupole moment much larger than the shell model prediction, which led them to claim the existence of a proton halo in this nucleus. The measurements of interaction cross section of Tanihata et al. [3] show no spectacular enhancement when compared to adjacent nuclei. A $(0+2)\hbar\omega$ shell model calculation by Nakada and Otsuka [4] suggests that the quadrupole momentum of ^{8}B can be explained without reference to a proton halo. Also the generator coordinate model (GCM) calculation of Descouvemont and Baye [5] shows no clear indication of a proton halo, while the resonating group model (RGM) multiconfiguration-multicluster calculation of Csoto [6] indicates a proton skin of 0.5 fm. It has been shown that the behaviour of the proton density distribution in ^{8}B at large distance can be important for the high energy component of the solar neutrino flux [1,7].

Different experiments could probe the wave function of the proton interacting with the ^{7}Be core at different distances. The angular distributions of elastic scattering can in principle give informations on the density distributions and the corresponding optical potentials.

In this work we present the measurement of ^{7}Be,$^{8}B+^{12}C$ quasielastic scattering at 40 MeV/nucleon. The scattering of $^{12}C+^{12}C$ at 20 MeV/nucleon was used to check the method of extracting angular distribution from the experimental data.

II. EXPERIMENTAL METHOD

Secondary beams of ^{8}B and ^{7}Be, with an energy of 40 MeV/nucleon, were produced by fragmentation of a 60 MeV/nucleon ^{13}C beam on a 2 mm ^{9}Be target. The fragmentation products were subsequently separated using the doubly-achromatic

spectrometer LISE3 [8]. The purity of the secondary beams was enhanced by the use of a 1120 μm aluminium wedge located in the first dispersive plane of LISE3.

The intensity of the ^{8}B beam was 700 pps and represented an optimum with respect to the pile-up effects. The purity of the ^{8}B secondary beam was better than 99.2%. The momentum acceptance of the spectrometer in this case was 1.1%. The ^{7}Be secondary beam had an intensity of 1000 pps, a momentum acceptance of 0.33% and a purity of 98.4%. Finally, a ^{12}C beam of 2200 pps was produced with the same ^{13}C primary beam to test and measure the efficiency of the experimental setup in a wide range of angles. The diameter of the beam spot on the secondary target was in all 3 cases about 7 mm FWHM.

The experimental setup, shown in fig. 1, was considerably improved compared to an earlier experiment performed with a ^{11}Li beam [9]. It consisted of two position sensitive (x,y) parallel-plate avalanche counters (PPAC) placed at a distance of about 1m from each other. The second PPAC was placed 42 mm away from the secondary target made of 18.5 mg/cm^2 of carbon. The position resolution of the PPAC's was 1.5 mm FWHM which ensured a measurement of the angle of secondary beam with an angular resolution better than 0.15 deg. Both PPACs provided also start signals for a time of flight (TOF) measurement between each PPAC and the radiofrequency of the cyclotron.

The scattered particles were detected by an assembly of three silicon strip detectors (E1, E2, E3) of 150μm, 500μm and 4500μm respectively. The E1 detector consists of 32 circular strips of 0.77 mm with a central hole of 15 mm diameter and an external diameter of 68 mm. The E2 detector has 32 radial strips within the same inner and outer diameters. The E3 detector has four radial sectors and served as a stop detector. The first two detectors also provided information on the energy loss which, in combination with the residual energy given by the third detector, was used for particle identification. However, the overall energy resolution (4 %) was not sufficient to fully distinguish between elastic and inelastic scattering. In order to increase the range of measured angles the assembly of E1, E2 and E3 detectors was placed during the

experiment at two different distances with respect to the target: 133 mm and 328 mm respectively . The two settings had a wide angular overlap, so that both extracted angular distributions could be compared with each other.

Downstream of the above assembly (see fig.1), a telescope consisting of 11 silicon detectors served simultaneously to measure the excitation function of the $^{8}B \longrightarrow {}^{7}Be+p$ break-up on silicon target. The results of the break-up of measurement will be presented in details in a forthcoming publication.

The measurement of energy losses in different detectors of the telescope allowed us to separate and count also the ^{7}Be nuclei coming from the break-up of ^{8}B on carbon target at 40 MeV/nucleon, giving a direct estimation of a break-up cross section.

Control measurements without secondary target were performed in order to determine the contribution of background events coming from beam scattering on materials other than the target. Their contribution turned out to be less than 2 %.

Extensive Monte Carlo simulations were performed in order to carefully evaluate the efficiency of the set-up. The incident secondary beam directions, defined on an event by event basis by the PPACs, was taken as input for the efficiency simulations. Then, the trajectories of the particles after the target were generated and intercepted on an exact image of the three detectors that included all inactive areas. In this way, the efficiency was obtained as a function of the measured angle for subsequent use in the cross section calculation. As the geometrical efficiency is an important factor for the data analysis, several requirements were imposed in the Monte Carlo simulation. The efficiency must depend only on geometrical structure of the system and not on the angular distribution used to generate the scattering angles. In this respect, several angular dependences of the generated elastic cross sections were tested.

The finite spatial resolution of the PPACs and of the strip detectors, as well as the multiple scattering and angular straggling in the target were taken into account to obtain the final angular resolution for each angle presented as horizontal error bars in fig.2.

Drastic conditions were imposed on the data analysis for the ^{8}B case. A minimum deflection of 2 deg (c.m.) (larger than the angular resolution by more than 3σ) was imposed to eliminate most of primary beam particles. Special care was taken in the analysis of PPAC's signals.

The ^{7}Be nuclei produced by a break-up reaction in the secondary target were clearly separated in the energy-loss spectra.

The data obtained in the present work are shown in fig.2. A comparison of ^{12}C scattering data with the previously reported pure elastic scattering data measured by Bohlen et al. [10] shows a good agreement. It should be emphazised that in the present experiment it was possible to measure elastic scattering down to 2 deg in the center-of-mass system.

III. QUASIELASTIC SCATTERING

In the following, the quasielastic data obtained in this work are interpreted in terms of the distorted-waves Born approximation (DWBA) and the coupled-channels (CC) approximations. Due to the restricted angular range and the considerable mixing of inelastic scattering, a direct fit to the data is difficult. We prefer to compare a semimicroscopic prediction for elastic and inelastic cross sections with the data.

The double folding model associated with the effective interaction of Jeukenne, Lejeune and Mahaux (JLM) [11] was chosen to construct the necessary elastic optical potentials and the form factors for inelastic scattering. These authors have proposed a complex, density and energy dependent interaction, derived in such a way that the entire nucleon-nucleus potential can be obtained with the Hartree term only. In extrapolating to heavy ions, the main difficulty arises from the ambiguity in the definition of density in the overlap region. Here, we have chosen the following approximation:

$$\rho(r_1,r_2)=[\rho_1(r_1).\rho_2(r_2)]^{1/2} \qquad (1)$$

which underestimates the density for strong overlaps but does not give rise to unphysical situations, as does the usual approximation: $\rho(r_1,r_2)=\rho_1(r_1)+\rho_2(r_2)$. Coulomb corrections were neglected because they are only important near the Coulomb barrier. The imaginary part has a correct behaviour near the Fermi surface and includes effective mass correction. Only the isoscalar components have been retained.

The diagonal part of the one body densities for ^{7}Be and ^{8}B in the **r** space have been obtained in a multiconfigurational shell-model (SM) calculation. The occupation probabilities were obtained by diagonalization of the Warburton-Brown interaction [12] in the first four major shells using the OXBASH code [13]. The spurious center of mass motion was removed by the usual method [14], by adding the center of mass Hamiltonian to the interaction. The first four major shells provide a completely nonspurious shell-model basis when $2\hbar\omega$ configurations are included. The residual interaction used in the shell model procedure does not fix the single particle wave functions (s.p.w.f.). We have chosen the Hartree-Fock (HF) s.p.w.f. as a basis, which seems to be more adequate to describe the nuclear surface. We used the Skyrme III force (SkIII) [15] and the occupation probabilities from the SM calculation as inputs to the HF program. For consistency, the ^{12}C one body density was obtained in a standard HF SkIII calculation.

As can be seen from table 1, the SM calculations predict a comparable proton skin for ^{7}Be and ^{8}B nuclei. The skin is defined as the difference between RMS radii of the proton and neutron distributions. These very diffuse densities may induce an increase of refraction effects in elastic scattering for both nuclei. However, we expect that the larger absorption in ^{8}B due to a smaller threshold for break-up will produce an additional damping of the ^{8}B elastic cross section.

The bare folding optical potential only contains two parameters: the normalization constants N_V and N_W for real and imaginary part, respectively. This normalization is necessary in order to compensate for the underestimation of density effects at large density overlap.

For the $^{12}C+^{12}C$ case, the interaction was fixed by fitting the original data of Bohlen et al. in a standard coupled channels (CC) calculation. The ^{12}C nucleus was treated as a rigid rotor and couplings involving both excitation and de-excitation between ground state (0^+) and first excited state (2^+,4.44 MeV) were used. The B(E2↑) value was taken from the compilation of Raman et al. [16] and the same deformation length was used for all components of the optical potential. With the normalization constants N_V=0.56 and N_W=0.84 the agreement with the data of Bohlen et al. is good, especially in the diffractive region (fig.3). The above results demonstrate that our folding potentials can be safely used to describe both elastic and inelastic scattering. This allows to diminish the ambiguities in the interpretation of ^7Be and ^8B quasielastic scattering.

The above calculation is also compared with our experimental data on $^{12}C+^{12}C$ quasielastic scattering (fig.4). The excitation of the 3^- state was calculated using the DWBA and vibrational model, with a deformation length δ_3 taken from ref. [17]. The inelastic scattering and finite angular resolution account well for the filling of the minima. The satisfactory agreement obtained with the $^{12}C+^{12}C$ data brings confidence in the method used for analysis of the data.

The same type of calculation has been performed for ^7Be and ^8B quasielastic scattering. In these cases the normalization constants N_V and N_W were obtained by fitting the pure elastic scattering of $^6Li+^{12}C$ at 26 MeV/nucleon, 35 MeV/nucleon and 53 MeV/nucleon [18,19,20]. All spurious solutions were eliminated by retaining only the smooth energy dependence of the normalization constants. Fits, as good as in the $^{12}C+^{12}C$ case, were obtained in the full angular range, including the so called rainbow region, which shows that our interaction has a correct behaviour well inside the strong absorption radius. The interpolated values for an energy of 40 MeV/nucleon are N_V=0.65 and N_W=0.80. The large reduction of the real part arises mainly from the underestimation of the density effects by the approximation (1). By taking the normalization constants from $^6Li+^{12}C$ scattering, a large part of the dynamical polarization potential (DPP) arising from the strong coupling to the break-up channel is already included in our potentials. As can be seen from fig.5a the agreement with the quasielastic data is good in the ^7Be case.

Both magnitude and oscillations are correctly reproduced. The excitation of the 2^+ state in ^{12}C accounts to a large extent for the filling of first deep minimum at 6.5 deg. Its contribution becomes comparable with the elastic scattering at angles larger than 10 deg. The 3^- excitation, although much smaller in amplitude, gives a non-negligible contribution at large angles.

The same type of CC calculation performed for ^8B quasielastic scattering is compared to the data in fig.5b. The agreement with the data is worse than in the ^7Be case. The structures shown by the data are less pronounced. The filling of the minima cannot be entirely explained by inelastic contribution from the target excitation. One might suspect an additional contribution from projectile excitation. In order to check this hypothesis, a separate CC calculation has been done to evaluate the contribution of a quasibound (1^+,0.77 MeV) level placed just above the ^7Be+p threshold. The reduced transition probability was taken from the GCM estimation of Descouvemont and Baye [5]. The inelastic cross section was added incoherently to the results of the preceding calculation. As can be seen on fig.6, projectile excitation does not significantly change the results.

The calculation presented on fig.6 shows still a discrepancy in the magnitude of cross section at angles corresponding to diffraction minima. All tests of other different optical potentials e.g. a double folding potential with M3Y interaction as well as a simple Woods-Saxon one resulted in even more pronounced minima comparing to the experimental data. These facts suggest that the data for the loosely bound nucleus ^8B cannot be entirely explained by optical model amplitudes. Similar discrepancies were found for elastic scattering of ^{11}Li on silicon [9] and carbon [21], where the cross section at small angles is underestimated by the optical model.

IV. REACTION CROSS SECTION

Further information can be obtained from reaction cross sections (see table 2). We compare our results denoted by JLM with the phenomenological formula of Kox [22] using the isospin component suggested by Zahar et al. [23]. The individual radii

were calculated from the liquid drop model parametrization used by Shen et al.[24]. In a subsequent calculation, the mean square radii from the present SM calculation were used for ^{7}Be and ^{8}B together with the SkIII value for ^{12}C. The JLM folding model predicts an increased absorption of 78 mb for ^{8}B. An experimental estimation of the break-up on ^{12}C target extracted directly from the independent measurement using the silicon telescope gives also σ_{-p}=80±15 mb. This value is consistent with the result of a Glauber type calculation using the two-body wave functions of Riisager and Jensen [1] and compares well with the break-up cross section (σ_{-p}) of 60±5 mb obtained by Corre [25] in an experiment for $^{8}B+^{28}Si \rightarrow ^{7}Be+p+^{28}Si$ at the same energy. This suggests an approximate factorization of the proton-core wave function and shows that a Glauber type relation

$$\sigma_{-p}=\sigma_R(^{8}B) - \sigma_R(^{7}Be) \qquad (2)$$

is also valid for the proton break-up of ^{8}B. The table includes the experimental interaction cross section obtained by Tanihata et al.[7] at 790 MeV/nucleon for completeness. The difference in the reaction cross section (about 8%) corresponds to an increase of the interaction radius of 4%. Tanihata et al. [3] obtained 3% at 790 MeV/nucleon. Therefore, the existence of a large halo in ^{8}B is not supported by the present data.

The rather small increase of the interaction radius obtained here could be understood in terms of an effective separation energy [26] which in our case amounts to:

$$S_{eff}=S_p+B_c \qquad (3)$$

where B_c is the Coulomb barrier and S_p=0.137 MeV. For ^{8}B, the Coulomb barrier contributes with about 6 MeV to the effective separation energy. Consequently the Coulomb barrier contributes largely to the confining of the last bound proton inside the nucleus volume, preventing the radius to get very large.

V. SEMICLASSICAL ANALYSIS

It is interesting to compare the pair of nuclei (^{7}Be,^{8}B) studied in the present paper and the pair (^{11}C,^{11}Li) recently analyzed by Hussein and Satchler [27]. On the basis of semiclassical arguments, they found that for loosely bound nuclei like ^{11}Li, the

increased extension of the one-body density (due to the halo) enhances the refractive power of the real optical potential. The corresponding enhancement of the elastic cross section is then compensated by the increased absorption due to the halo. Also, the strong coupling with the break-up channel gives rise to an additional damping of elastic cross section, through the long tail of the imaginary part of the induced dynamical polarization potential (DPP). The presumably repulsive real part of the DPP gives rise to smaller damping at large angles.

We have checked these ideas for the present data. A farside-nearside decomposition of the elastic cross section is presented in fig.7. Beyond the cross-over angle, both cross sections are farside dominated, but the farside component decreases much faster for ^{8}B than for ^{7}Be at large angles. According to Hussein and Satchler [27] this effect may be attributed to an increased imaginary part of the complex angular momentum in the ^{8}B case.

Additional information can be obtained from optical model absorption profiles (fig.8a) and the WKB deflection functions (fig.8b). In both figures, the curves correspond to the bare JLM folding potential. The bright side of the deflection function is similar in these two cases, while the dark component is slightly more diffuse for ^{8}B. The rainbow angle $\theta_R \sim$ -30 deg corresponds to an angular momentum $\lambda_R \sim 20\hbar$. As can be seen from the absorption profiles, the rainbow effect in the cross section is removed by the strong absorption corresponding to trajectories with $\lambda < \lambda_R$. Beyond the crossover angle, the cross section is dominated by the $\lambda_>$ branch of the deflection function. Since $\lambda_>(^{7}\text{Be}) < \lambda_>(^{8}\text{B})$ the cross section for ^{8}B appears more damped than for ^{7}Be at these angles.

VI. SUMMARY

The quasielastic scattering of ^{7}Be and ^{8}B at 40 MeV/nucleon on ^{12}C target has been measured for the first time. The experimental method was carefully tested by comparing our ^{12}C+^{12}C (20 MeV/nucleon) measurement with the existing data of Bohlen et al. [10]. Extensive Monte Carlo simulation has been done to extract the geometrical

efficiency of the setup and to estimate the experimental error bars. Shell model one-body densities and the effective interaction of Jeukenne, Lejeune and Mahaux [11] were used to generate the elastic optical potentials and the form factors for inelastic scattering. Our SM calculation for one body densities predicts a significant proton skin for both ^{7}Be and ^{8}B nuclei. The normalization constants of the effective interaction extrapolated from ^{6}Li+^{12}C data at similar energy and coupled-channels (CC) calculations account well for the quasielastic scattering data of ^{7}Be. The CC calculation for the ^{8}B nucleus does not reproduce satisfactorily the quasielastic scattering data. As in the ^{11}Li case it is difficult to reproduce the small angle cross section with a simple optical model. In spite of these difficulties, an agreement of the one proton removal cross section calculated by formula (3) with an experimental value of the break-up cross section can be noticed. The obtained value (σ_{-p}~80 mb) does not support a proton halo hypothesis for the ^{8}B nucleus.

The semiclassical analysis revealed for ^{8}B a number of similarities with ^{11}Li resulting from a combined effects of proton and/or neutron skin and of the low threshold for break-up. The stronger Coulomb interaction in ^{8}B confines the proton wave function in the nuclear interior and inhibits the existence of proton halo. The folding potentials generated by the JLM microscopic effective interaction (which has a proper mass and energy dependence) are much stronger for ^{8}B than for ^{7}Be in both real and imaginary parts. The increased refraction is masked by the stronger absorptive part of the potential and the resulting ^{8}B elastic cross section appears much damped at large angles compared to the ^{7}Be.

ACKNOWLEDGEMENTS

We are very indebted to Dr. M.Horoi for providing us with the SM occupation numbers and to Dr. A.Nadasen, Dr. H.Bohlen and Prof. H.Rebel for numerical elastic cross sections data. Technical support of R.Hue and F.Geoffroy is also acknowledged. One of the authors (A.Kordyasz) acknowledges financial support from The State Committee for Scientific Research under grant No 2P302 215 04.

REFERENCES

[1] K.Riisager and A.S.Jensen, Phys. Lett. B**301**, 6 (1993)

[2] T.Minamisono et al., Phys. Rev Lett. **69**, 2058 (1992)

[3] I.Tanihata, H.Hamagaki, O.Hashimoto, Y.Shida, N.Yoshikawa, K.Sugimoto, O.Yamakawa, T.Kobayashi and N.Takahashi, Phys. Rev. Lett. **55**, 2676 (1985); I.Tanihata, T.Kobayashi, O.Yamakawa, T.Shimoura, K.Ekuni, K.Sugimoto, N.Takahashi, T.Shimoda, H.Sato, Phys. Lett. B**206**, 592 (1988)

[4] H.Nakada and T.Otsuka, Phys. Rev. C**49**, 886 (1994)

[5] P.Descouvemont and D.Baye, Nucl. Phys. **A567**, 341 (1994)

[6] A.Csoto, Phys Lett. B**315**, 24 (1993)

[7] J.N.Bahcall, W.F.Huebner, S.H.Lubow, P.D.Parker and R.K.Ulrich, Rev. Mod. Phys. **54**, 767 (1982)

[8] R.Anne and A.C.Mueller, Nucl.Instr.Meth. B**70**, 276 (1992)

[9] M.Lewitowicz et al., Nucl. Phys. **A562**, 301 (1993)

[10] H.G.Bohlen et al., Z. Phys. A**322**, 241 (1985)

[11] J.-P.Jeukenne, A.Lejeune and C.Mahaux, Phys. Rev. C**16**, 80 (1977)

[12] E.K.Warburton and B.A.Brown, Phys. Rev. C**46**, 923 (1992)

[13] B.A.Brown et al., MSUNSCL Report, **524** (1988)

[14] D.H.Gloeckner and R.D.Lawson, Phys. Lett. B**53**, 313 (1974)

[15] M.Beiner, H.Flocard, Nguyen van Giai and P.Quentin, Nucl. Phys. **A238**, 28 (1975)

[16] S.Raman, C.W.Nestor, Jr., S.Kahane and K.H.Bhatt, At.Data & Nucl.Data Tables **42**, 1 (1989)

[17] R.H.Spear, At.Data & Nucl.Data Tables **42**, 55 (1989)

[18] J.Cook,H.J.Gils,H.Rebel,Z.Majka and H.Klewe-Nebenius,KfK **3233** (1981)

[19] A.Nadasen et al., Phys Rev. C**37**, 132 (1988)

[20] A.Nadasen et al., Phys Rev. C**47**, 674 (1993)

[21] J.J.Kolata et al., Phys. Rev. Lett. B**69**, 2631 (1992)

[22] S.Kox et al., Phys. Rev. C**35**, 1678 (1987)

[23] M.Zahar et al., Phys. Rev C**49**, 1540 (1994)

[24] Shen Wen-qing, Wang Bing, Feng Jun, Zhan Wen-long, Zhu Yong-tai and Feng En-pu, Nucl. Phys. **A491**, 130 (1989)

[25] J.-M.Corre, Thesis

[26] M.Lassaut and R.J.Lombard, Preceedings of 6th Int. Conf. on Nuclei Far From Stability & 9th Int. Conf. on Atomic Masses and Fundamental Constants, Bernkastel-Kues, 1992

[27] M.S.Hussein and G.R.Satchler, Nucl. Phys. **A567**, 165 (1994)

Figure captions.

Figure 1.
Schematic diagram of the experimental setup.

Figure 2.
Quasielastic scattering of ^{7}Be (40 MeV/nucleon), ^{8}B (40 MeV/nucleon) and ^{12}C (20 MeV/nucleon) on a ^{12}C target in the center of mass system. The vertical error bars indicate a statistical uncertainty, the horizontal ones were estimated from the widths of strips in E1 and E2 detectors and a spatial resolution of PPACs. The solid line indicates the elastic scattering of ^{12}C on the ^{12}C target measured by Bohlen et al. [10].

Figure 3.
Coupled-channels calculation of a) elastic and b) inelastic (2+) scattering (solid lines) compared with the experimental data of Bohlen et al. [10] (points).

Figure 4.
Coupled-channels calculation of the elastic (thin solid line) and the inelastic (2^{+}) (dashed line) scattering. The contribution of the (3^{-}) state of ^{12}C is calculated in DWBA (dotted line). The incoherent sum of elastic and both inelastic channels (thick solid line) is compared with experimental data (points). An experimental angular resolution was taken into account in the calculations.

Figure 5.
Quasielastic scattering of a) ^{7}Be and b) ^{8}B on ^{12}C target. The coupled-channels calculation of elastic (thin solid line) and inelastic (2^{+}) (dashed line) scattering are presented. The contribution of the (3^{-}) state of ^{12}C is calculated in DWBA (dotted line). The incoherent sum of elastic and both inelastic channels (thick solid line) is compared with experimental data (points). An experimental angular resolution was taken into account in the calculations.

Figure 6.
Same as fig.5b except that the dashed line indicates the sum of elastic and both inelastic channels, the dotted line indicates the scattering to an excited state (1^{+}) of ^{8}B and the solid line is the sum of all these channels.

Figure 7.

Farside-nearside decomposition for elastic scattering of a) ^{7}Be and b) ^{8}B on ^{12}C. The dashed (dotted) lines correspond to farside (nearside) components. The solid lines correspond to the sum of both components, the points indicate the experimental data.

Figure 8.

a) Optical model absorption profiles. The arrows indicate the conventional strong absorption angular momentum.b) WKB deflection functions. The solid line corresponds to ^{8}B, the dashed one to ^{7}Be.

Table captions.

Table I.

Characteristics of nuclear densities. Root mean square radii of densities for JLM folding potential are presented. Different radii for protons $\langle r_p^2 \rangle^{1/2}$, neutrons $\langle r_n^2 \rangle^{1/2}$ and whole nuclei $\langle r_m^2 \rangle^{1/2}$ are compared. $\langle r_p^2 \rangle^{1/2} - \langle r_n^2 \rangle^{1/2}$ indicates the difference between r.m.s. radii for protons and neutrons.

Table II.

Reaction cross sections. Predictions given by: a) JLM folding model, b) Kox-type formula as modified by Zahar et al. [23], c) the same as b) but for radii presented in Table 1., d) experimental values at 790 MeV/nucleon obtained by Tanihata et al. [3].

Table I

	$\langle r_p^2 \rangle^{1/2}$ (fm)	$\langle r_n^2 \rangle^{1/2}$ (fm)	$\langle r_m^2 \rangle^{1/2}$ (fm)	$\langle r_p^2 \rangle^{1/2} - \langle r_n^2 \rangle^{1/2}$ (fm)	density
^{7}Be	2.337	2.108	2.242	0.229	SM
^{8}B	2.400	2.068	2.281	0.332	SM
^{12}C	2.423	2.398	2.410	0.020	SKIII

Table II

	Reaction cross section (mb)	
	^{7}Be+^{12}C	^{8}B+^{12}C
JLM[a)]	1026	1104
Kox [b)]	1037	1186
Kox [c)]	1062	1179
Tanihata [d)]	738±9	784±14

Figure 1

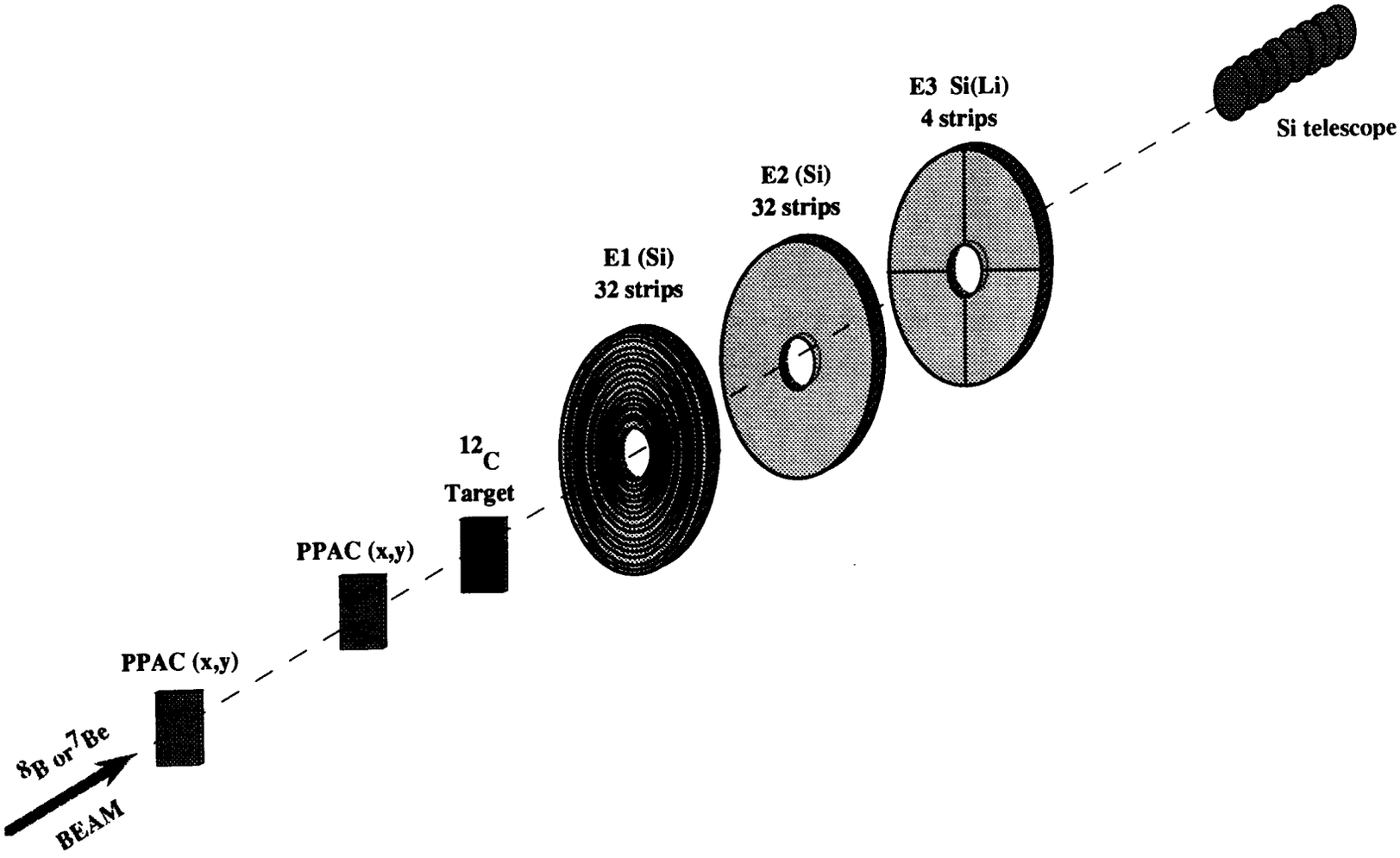
E3 Si(Li)
4 strips
Si telescope
E2 (Si)
32 strips
E1 (Si)
32 strips
12C
Target
PPAC (x,y)
PPAC (x,y)
8B or 7Be
BEAM

Figure 2

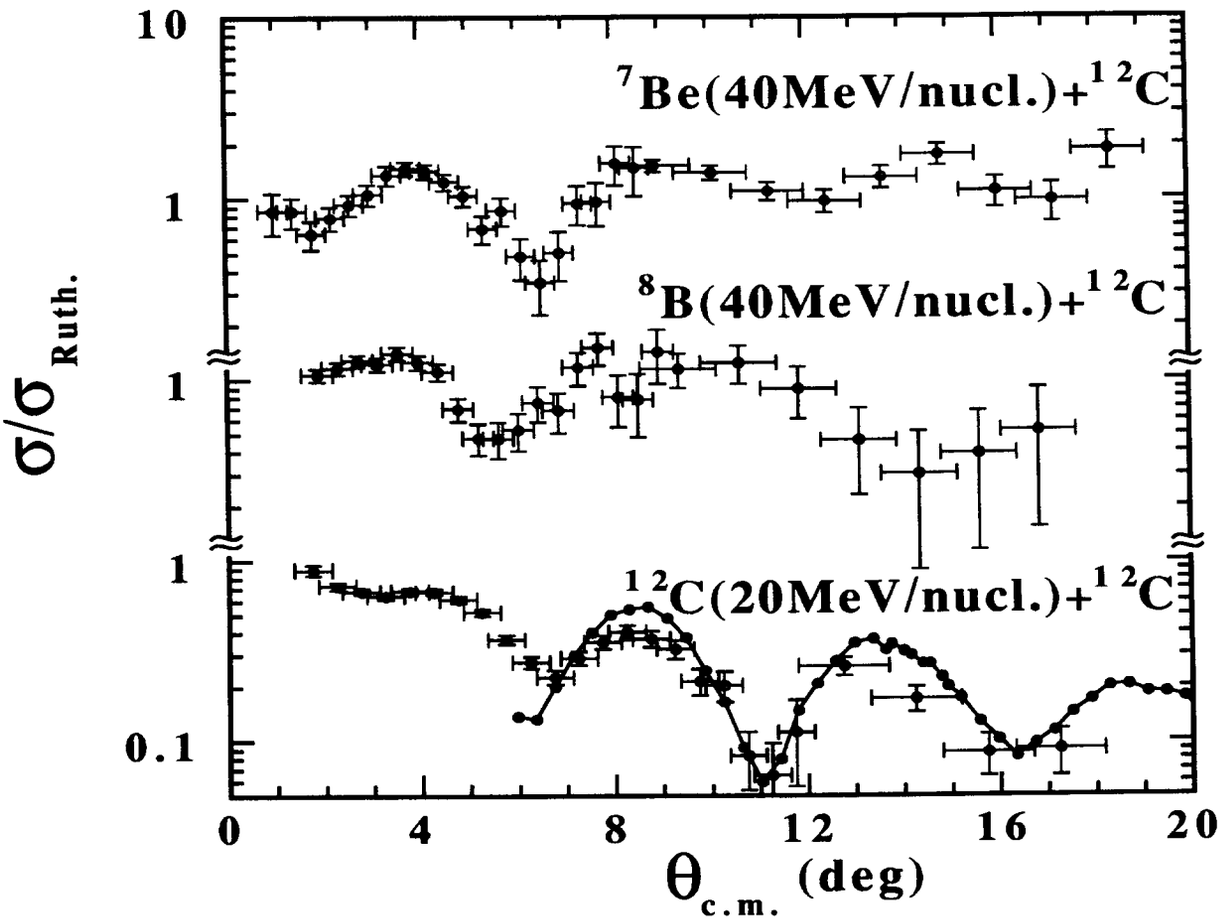
10
1
1
1
0.1
σ/σ Ruth.
7Be(40MeV/nucl.)+12C
8B(40MeV/nucl.)+12C
12C(20MeV/nucl.)+12C
0
4
8
12
16
20
θc.m. (deg)

Figure 3

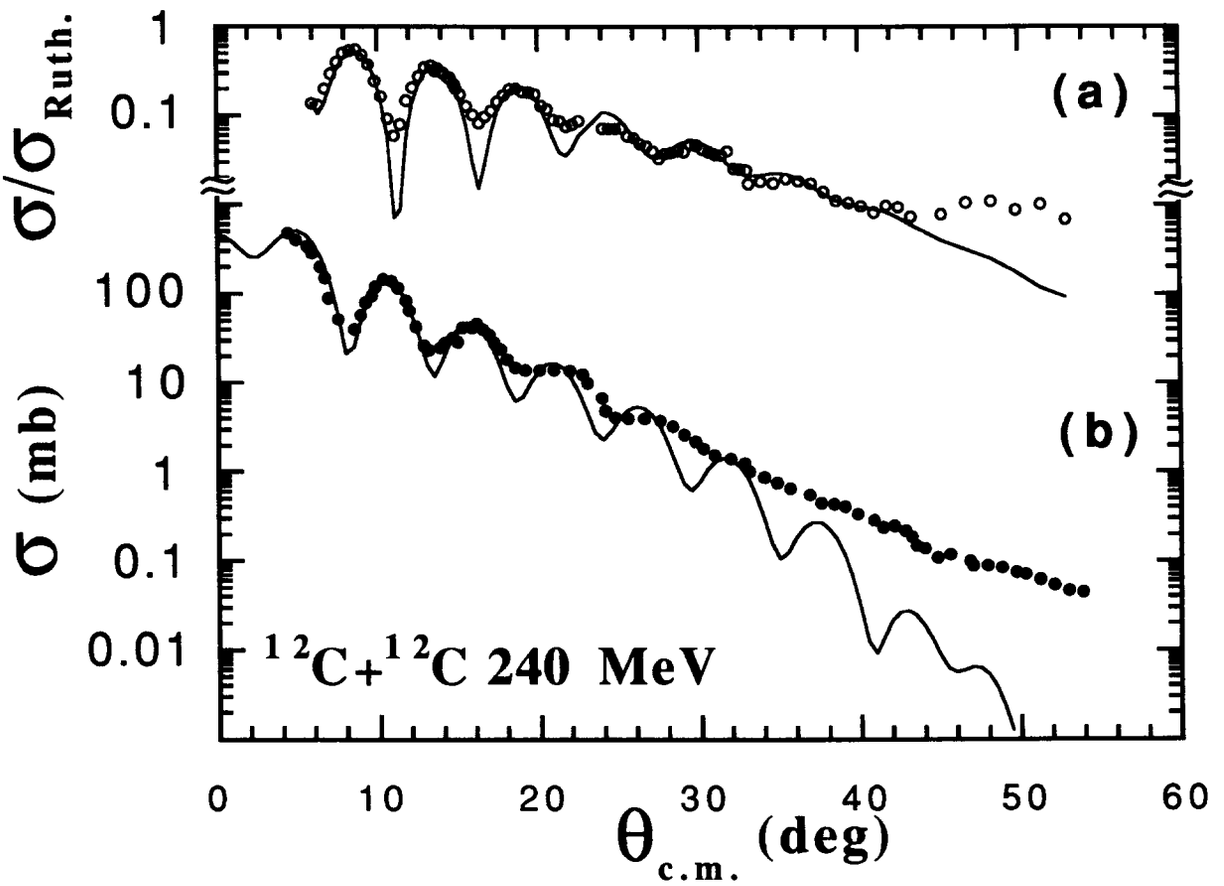
σ/σ Ruth.
1
0.1
(a)
100
10
1
0.1
0.01
σ (mb)
(b)
12C+12C 240 MeV
0
10
20
30
40
50
60
θc.m. (deg)

Figure 4

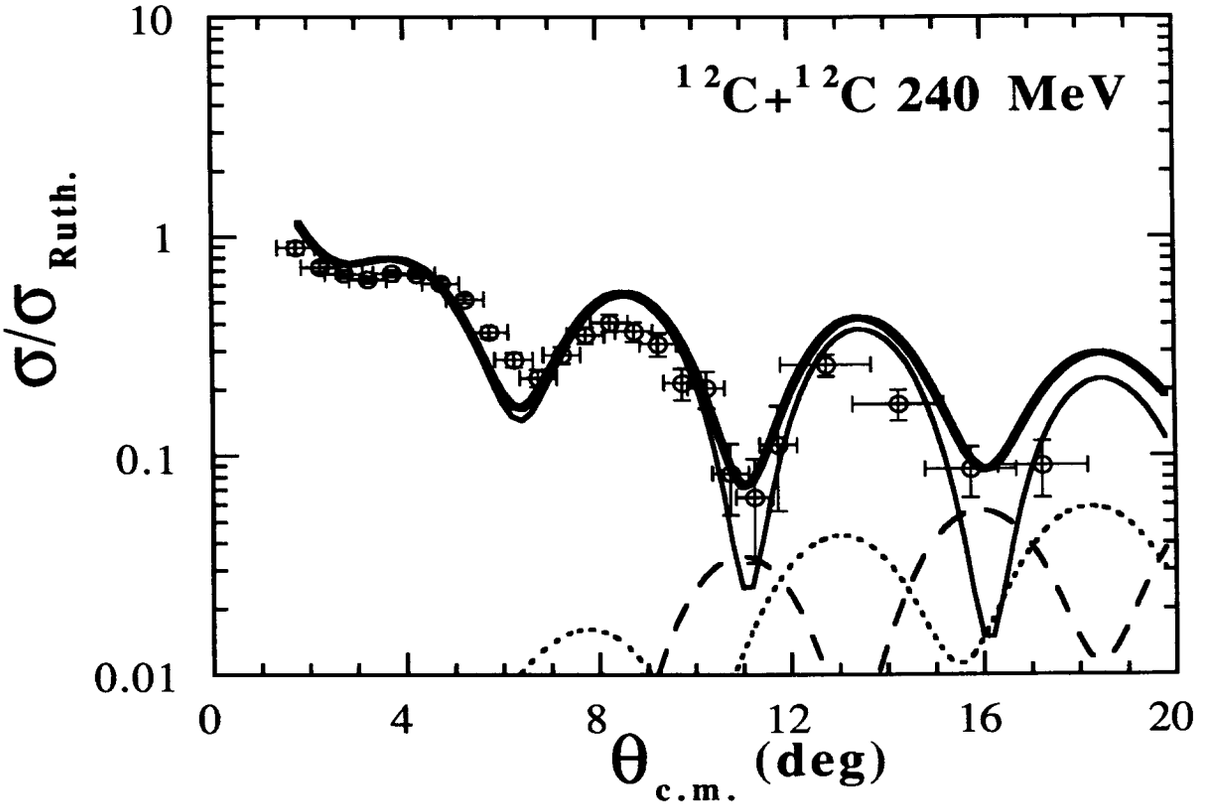

Figure 5

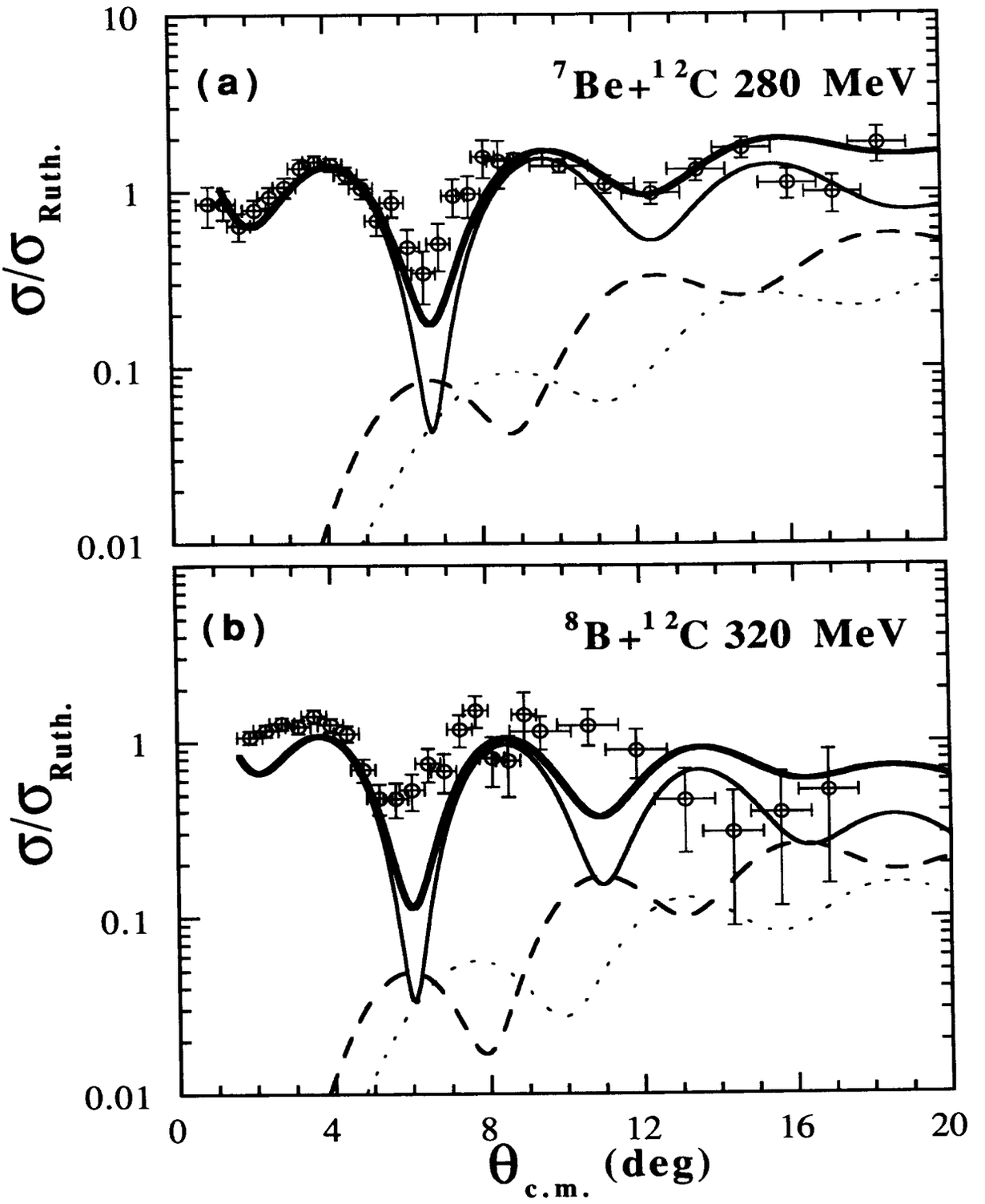
(a)
$^{7}Be+^{12}C$ 280 MeV
(b)
$^{8}B+^{12}C$ 320 MeV
$\sigma/\sigma_{Ruth.}$
10
1
0.1
0.01
0
4
8
12
16
20
$\theta_{c.m.}$ (deg)

Figure 6

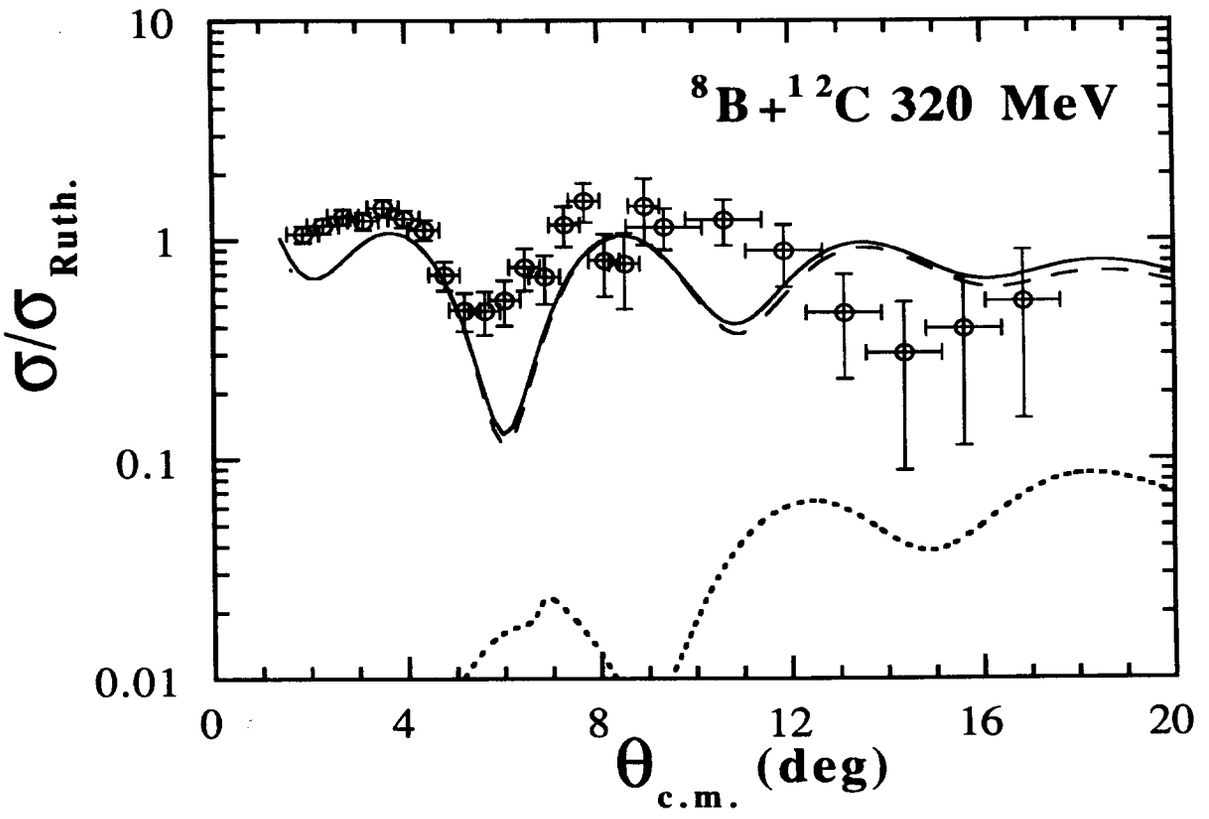
$^{8}B + ^{12}C$ 320 MeV
$\sigma/\sigma_{Ruth.}$
10
1
0.1
0.01
0
4
8
12
16
20
$\theta_{c.m.}$ (deg)

Figure 7

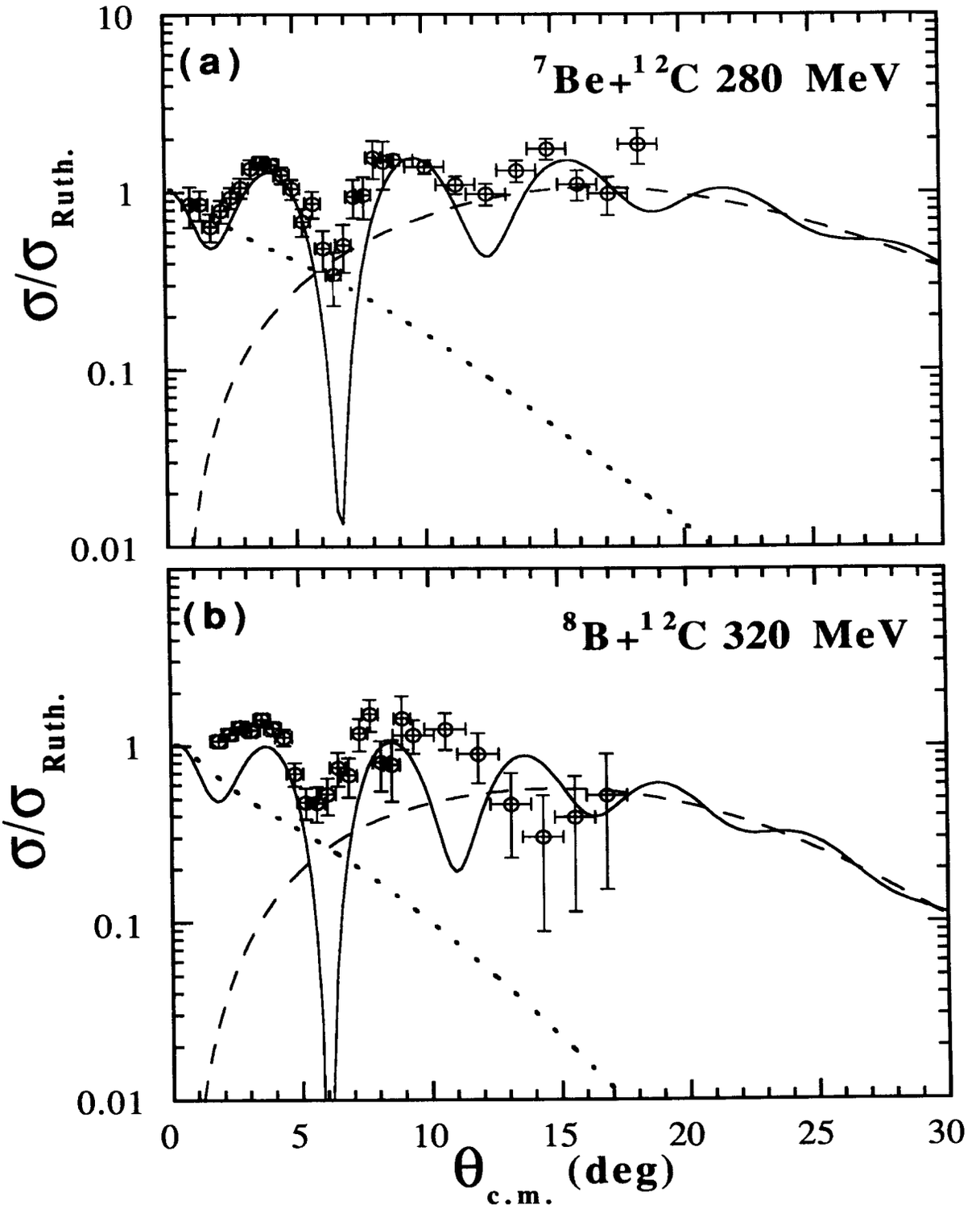
(a)
$^{7}Be+^{12}C$ 280 MeV
(b)
$^{8}B+^{12}C$ 320 MeV
$\sigma/\sigma_{Ruth.}$
10
1
0.1
0.01
0
5
10
15
20
25
30
$\theta_{c.m.}$ (deg)

Figure 8

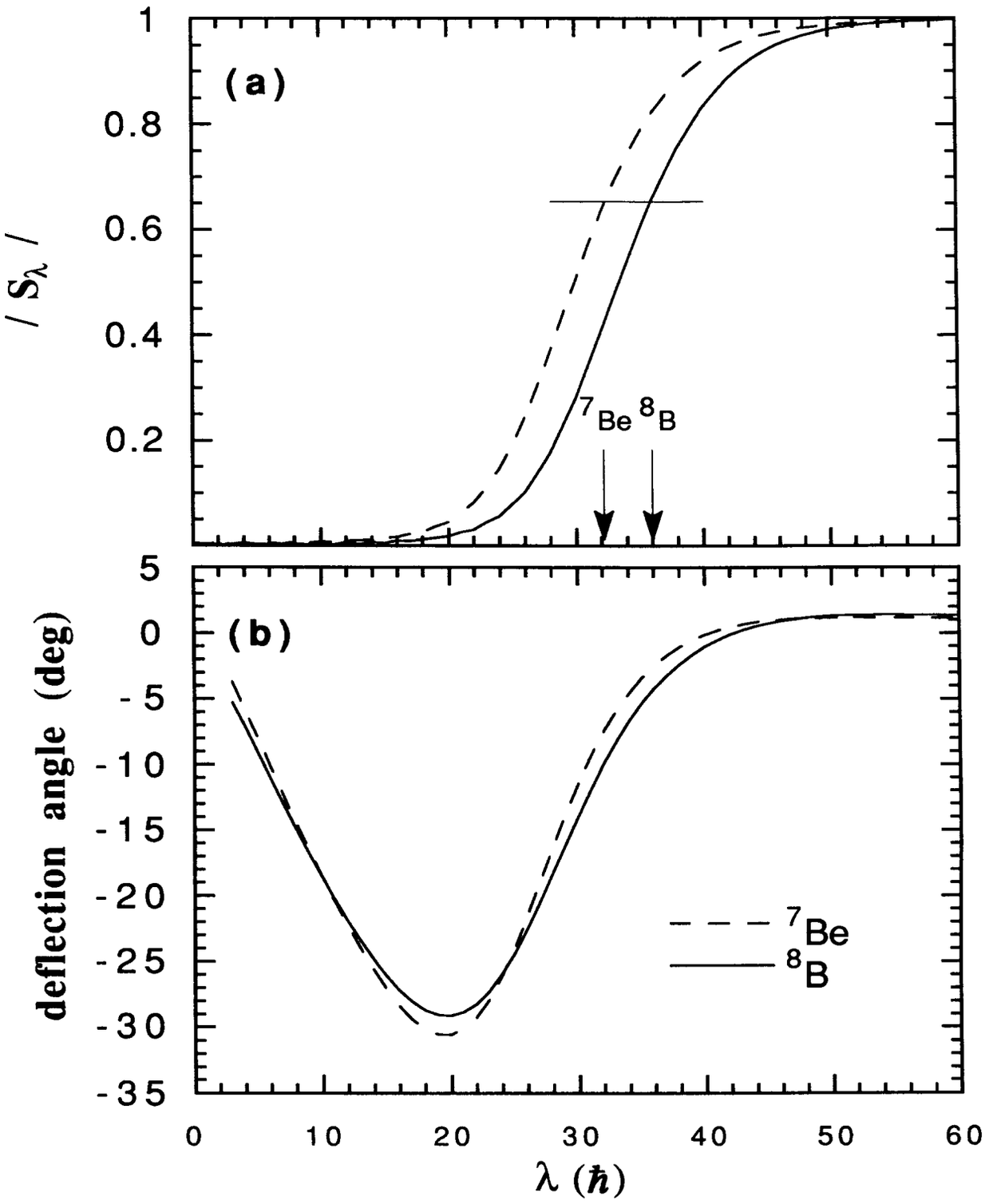
(a)
(b)
/ S_λ /
deflection angle (deg)
λ ($\hbar$)
^{7}Be
^{8}B
^{7}Be ^{8}B
1
0.8
0.6
0.4
0.2
5
0
-5
-10
-15
-20
-25
-30
-35
0
10
20
30
40
50
60